REPORT DOCUMENTATION PAGE

Form Approved OMB NO. 0704-0188

1. REPORT DATE (DD-MM-YYYY)	2. REPORT TYPE	3. DATES COVERED (From - To)
22-12-2008	Final Report	19-Jun-2007 - 31-Mar-2008

4. TITLE AND SUBTITLE
FINAL REPORT 2008 for STIR: ENCAPSULATING REACTIVE NANOPARTICLES IN CARBON NANOTUBES USING FLAME-BASED SYNTHESIS

5a. CONTRACT NUMBER
W911NF-07-1-0425

5b. GRANT NUMBER

5c. PROGRAM ELEMENT NUMBER
611102

6. AUTHORS
Stephen Tse

5d. PROJECT NUMBER

5e. TASK NUMBER

5f. WORK UNIT NUMBER

7. PERFORMING ORGANIZATION NAMES AND ADDRESSES
Rutgers, The State University of New Jersey - Pis
Office Of Research & Sponsored Programs
58 Bevier Road
Piscataway, NJ 08854 -8010

8. PERFORMING ORGANIZATION REPORT NUMBER

9. SPONSORING/MONITORING AGENCY NAME(S) AND ADDRESS(ES)
U.S. Army Research Office
P.O. Box 12211
Research Triangle Park, NC 27709-2211

10. SPONSOR/MONITOR'S ACRONYM(S)
ARO

11. SPONSOR/MONITOR'S REPORT NUMBER(S)
53052-CH-II.1

12. DISTRIBUTION AVAILIBILITY STATEMENT
Approved for Public Release; Distribution Unlimited

13. SUPPLEMENTARY NOTES
The views, opinions and/or findings contained in this report are those of the author(s) and should not contrued as an official Department of the Army position, policy or decision, unless so designated by other documentation.

14. ABSTRACT
The objective of this project is to study the feasibility of encapsulating nanoparticles with high aluminum content within carbon nanotubes (CNTs) during flame synthesis. In this manner, CNTs may be used to contain/store energetic nanomaterials, such that the resultant propellant/explosive not only possesses ameliorated stability and storage attributes, but also has the same (or enhanced) energy release characteristics. With respect to the gas-phase flow field and its impact on producing such nanomaterials, the effects of fuel composition, flame temperature, inert

15. SUBJECT TERMS
Carbon nanotube, energetics

16. SECURITY CLASSIFICATION OF:			17. LIMITATION OF ABSTRACT	15. NUMBER OF PAGES	19a. NAME OF RESPONSIBLE PERSON
a. REPORT	b. ABSTRACT	c. THIS PAGE			Stephen Tse
U	U	U	SAR		19b. TELEPHONE NUMBER 732-445-0449

Report Title

FINAL REPORT 2008 for STIR: ENCAPSULATING REACTIVE NANOPARTICLES IN CARBON NANOTUBES USING FLAME-BASED SYNTHESIS

ABSTRACT

The objective of this project is to study the feasibility of encapsulating nanoparticles with high aluminum content within carbon nanotubes (CNTs) during flame synthesis. In this manner, CNTs may be used to contain/store energetic nanomaterials, such that the resultant propellant/explosive not only possesses ameliorated stability and storage attributes, but also has the same (or enhanced) energy release characteristics. With respect to the gas-phase flow field and its impact on producing such nanomaterials, the effects of fuel composition, flame temperature, inert addition, hydrogen addition, oxygen concentration, and aerodynamic strain rate are investigated. With respect to the catalytic substrate, metal alloys and metal-oxide spinels are compared. It is anticipated that the study will help to determine local gas-phase conditions that will allow nanoparticles to be shed off at a given rate and encapsulated within the CNTs, along with the catalytic substrate properties (e.g. degree of crystallization in metal-oxide spinels) that will affect nanoparticle spacing and size.

List of papers submitted or published that acknowledge ARO support during this reporting period. List the papers, including journal references, in the following categories:

(a) Papers published in peer-reviewed journals (N/A for none)

Number of Papers published in peer-reviewed journals: 0.00

(b) Papers published in non-peer-reviewed journals or in conference proceedings (N/A for none)

Number of Papers published in non peer-reviewed journals: 0.00

(c) Presentations

"Gas-phase Synthesis of Nanoparticles, Nanotubes, and Nanowires for Energetic Applications," Gordon Research Conference on Energetic Materials, Tilton School, Tilton, NH, Jun 19, 2008.

Number of Presentations: 1.00

Non Peer-Reviewed Conference Proceeding publications (other than abstracts):

Tse, S.D., “Flame and Plasma Synthesis of Nanoparticles, Nanotubes, and Nanowires,” Corning/Rutgers Research Symposium, Corning, NY, Feb 25, 2008.

Zak, A., D’Esposito, C., and Tse, S.D., Premixed Flame Synthesis of Carbon Nanotubes,” W-I-P poster 32nd International Symposium on Combustion, The Combustion Institute, Aug 3-8, 2008, McGill University, Montreal, Canada.

Number of Non Peer-Reviewed Conference Proceeding publications (other than abstracts): 2

Peer-Reviewed Conference Proceeding publications (other than abstracts):

Number of Peer-Reviewed Conference Proceeding publications (other than abstracts): 0

(d) Manuscripts

Number of Manuscripts: 0.00

Number of Inventions:

Graduate Students

NAME	PERCENT_SUPPORTED
Cassandra D'Esposito	0.25
Megan Smith	0.25
Alexander Zak	0.10
FTE Equivalent:	**0.60**
Total Number:	**3**

Names of Post Doctorates

NAME	PERCENT_SUPPORTED
Sun, Geliang	0.30
FTE Equivalent:	**0.30**
Total Number:	**1**

Names of Faculty Supported

NAME	PERCENT_SUPPORTED	National Academy Member
Stephen Tse	0.10	No
FTE Equivalent:	**0.10**	
Total Number:	**1**	

Names of Under Graduate students supported

NAME	PERCENT_SUPPORTED
FTE Equivalent:	
Total Number:	

Student Metrics

This section only applies to graduating undergraduates supported by this agreement in this reporting period

The number of undergraduates funded by this agreement who graduated during this period:	0.00
The number of undergraduates funded by this agreement who graduated during this period with a degree in science, mathematics, engineering, or technology fields:.....	0.00
The number of undergraduates funded by your agreement who graduated during this period and will continue to pursue a graduate or Ph.D. degree in science, mathematics, engineering, or technology fields:.....	0.00
Number of graduating undergraduates who achieved a 3.5 GPA to 4.0 (4.0 max scale):	0.00
Number of graduating undergraduates funded by a DoD funded Center of Excellence grant for Education, Research and Engineering:	0.00
The number of undergraduates funded by your agreement who graduated during this period and intend to work for the Department of Defense	0.00
The number of undergraduates funded by your agreement who graduated during this period and will receive scholarships or fellowships for further studies in science, mathematics, engineering or technology fields:	0.00

Names of Personnel receiving masters degrees

NAME
Megan Smith
Alexander Zak
Total Number: **2**

Names of personnel receiving PHDs

NAME

Total Number:

Names of other research staff

NAME PERCENT_SUPPORTED

FTE Equivalent:

Total Number:

Sub Contractors (DD882)

Inventions (DD882)

FINAL REPORT 2008

STIR: ENCAPSULATING REACTIVE NANOPARTICLES IN CARBON NANOTUBES USING FLAME-BASED SYNTHESIS

(Grant # W911NF-07-1-0425)

Principal Investigator: Stephen D. Tse
Department of Mechanical and Aerospace Engineering, Rutgers University

SUMMARY

The objective of this project is to study the feasibility of encapsulating nanoparticles with high aluminum content within carbon nanotubes (CNTs) during flame synthesis. In this manner, CNTs may be used to contain/store energetic nanomaterials, such that the resultant propellant/explosive not only possesses ameliorated stability and storage attributes, but also has the same (or enhanced) energy release characteristics. With respect to the gas-phase flow field and its impact on producing such nanomaterials, the effects of fuel composition, flame temperature, inert addition, hydrogen addition, oxygen concentration, and aerodynamic strain rate are investigated. With respect to the catalytic substrate, metal alloys and metal-oxide spinels are compared. It is anticipated that the study will help to determine local gas-phase conditions that will allow nanoparticles to be shed off at a given rate and encapsulated within the CNTs, along with the catalytic substrate properties (e.g. degree of crystallization in metal-oxide spinels) that will affect nanoparticle spacing and size.

DESCRIPTION OF FINDINGS

Introduction

Energetic materials constitute an important part of the high-performance weaponry, e.g. propulsion and explosives systems, used by the U.S. Army. Recently, researchers have found that nanoscale energetic materials have the potential for enhanced energy release and mechanical properties, versus their conventional counterparts. Moreover, nanoenergetics can have higher energy density, providing reduced logistics burden (e.g. lower fuel and propellant usage).

An area of strong interest for the Army is in energetic nanomixtures and nanocomposites, which are mixtures/composites of nanopowder-based reactants that manifest high exothermic characteristics.[1] Thermite reactions, i.e. aluminothermic reactions in which aluminum metal is oxidized by the oxide of another metal, often make up these formulations, which can include Al/MoO_3, Al/CuO, Al/WO_3, Al/Fe_2O_3, Al/Bi_2O_3, and Al/MnO_2. See Fig. 1. Based on intermolecular, rather than intramolecular, reactions, energetic nanocomposites require intimate mixing of the reactants on the nanometer length scale, along with typical particle sizes in the tens of nanometers range (e.g. 30 nm).[1] The use of nanoscale particles enhance chemical kinetics due to their high surface area (> 100 times that of micron-sized particles used in traditional formulations) and short diffusion length.[2] Given the proximity and uniformity of the fuel and oxidizer nanostructures, the final nanophase composite can be extremely dense in energy and capable of generating high power.

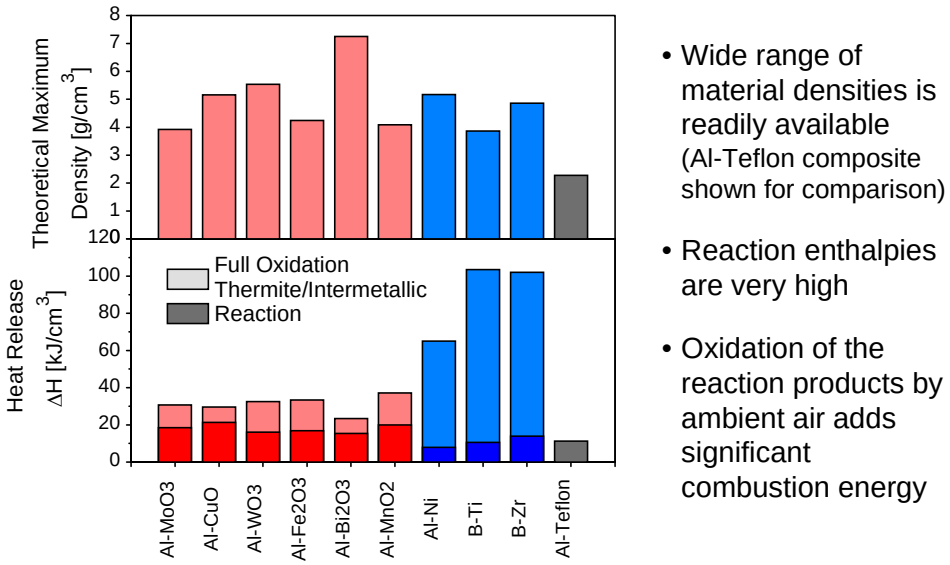

Figure 1. Densities and Reaction Enthalpies (from E. Dreizin, NJIT).

An essential aspect of producing successful nanoscale energetic materials is the ability to synthesize aluminum particles of diameters less than 50 nm, with an appropriately narrow size distribution. Reproducibility is critical, where batch-to-batch inconsistencies must be eliminated; and the manufacturing process should be amenable for mass production. These obstacles have yet to be sufficiently surmounted by present suppliers of such nanomaterials.

However, a key challenge in the application of nanodimensional fuels and oxidizers is the attainment of long-term passivation of the particle surface without losing the benefits of the faster reaction rate.[2] Presently, aluminum nanoparticles are passivated by oxide layers on their outer surfaces; however, this results in energy loss, decreased reactivity, and additional dead weight. Apart from performance (e.g. energy density, rate of energy release), the passivation process should ensure long-term storage stability and unwanted ignition (e.g. due to impact, friction, and electrostatic discharge). In these aspects, it is anticipated that CNTs may be used to encapsulate nanoscale energetics to deliver a propellant/explosive that not only has ameliorated stability and storage attributes, but also possesses the same (or enhanced) performance for energy release.[1] Unlike an oxide passivation layer, CNTs themselves can release energy. Works by Ajayan et al.[3] and Bockrath et al.[4] have demonstrated photoignition and burning of CNTs. See Fig. 2. Although the ignition mechanism is still not well understood, the authors hypothesize that heat confinement and photophysical effects associated with well-dispersed metal catalysts in intimate chemical contact with a high-surface-area carbon contribute to the phenomenon. Nonetheless, depending on the degree of sample compaction (with more bundles in contact with each other), the needed ignition power can be quite high, due to heat dissipation into the bulk sample by the highly conductive CNTs.[3] As a result, the CNTs can also provide a significant energy barrier for unwanted ignition of the embedded reactive nanoparticles. Thus, the objective of the present work is to study the feasibility of encapsulating aluminum nanoparticles within CNTs during simultaneous growth using a robust flame synthesis process.

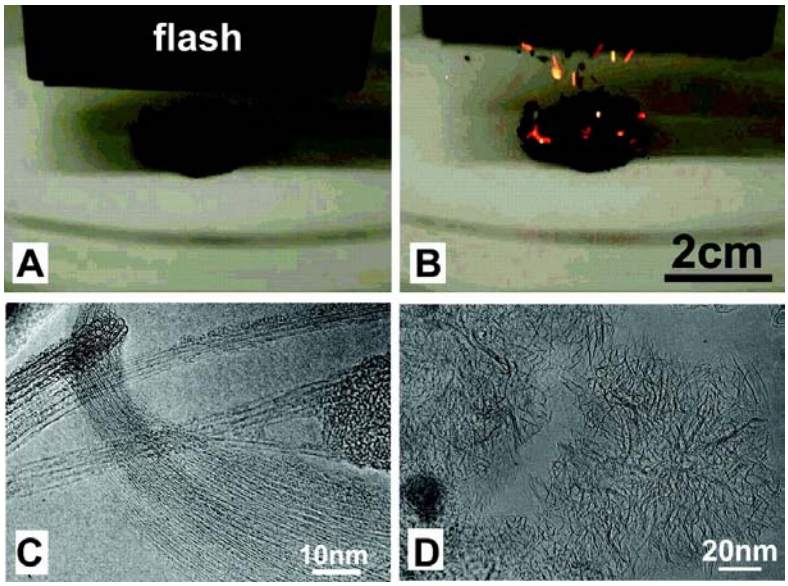

Figure 2. Combustion of Single-Wall Carbon Nanotubes (from Ref. 3).

Brief CNT Growth Background

Combustion synthesis has demonstrated a history of scalability and offers the potential for mass production, at reduced costs. The PI has been successful in synthesizing CNTs using combustion-based configurations, which possess an inherently cheaper source of process heat than any other technique and are already widely used to produce commercial carbon products. In utilizing combustion, the hydrocarbon gas provides both the high temperatures required as well as the hydrocarbon and CO reagents, thereby constituting an efficient synthesis process for CNTs. Moreover, the flame geometries utilized by the PI are quasi-one-dimensional, allowing for precise experimental probing, comparisons with simulations involving detailed gas-phase chemical kinetics and transport, and deduction of fundamental controlling mechanisms.

In the synthesis of CNTs, a well-accepted growth mechanism[5], as shown in Fig.3, incorporates adsorption, diffusion, and precipitation processes, with all occurring for given temperatures and chemical species. Parenthetically, other mechanisms such as the vapor-liquid-solid mechanism[6] and the yarmulke (skull-cap) mechanism[7] have been proposed, but will not be discussed here Given the presence of a catalytic transition metal (e.g. Fe, Ni, Co), these steps involve (a) hydrocarbon deposition and decomposition on the metal nanoparticle, (b) carbon migration diffusion through the particle, and (c) precipitation to form the CNT. CNTs can grow by the particle at the tip mechanism (Fig. 3(b)) or the particle at the base mechanism (Fig. 3(c)). However, it seems that the particle at the base mechanism would be most conducive for encapsulating nanoparticles within the CNTs, as particles may be periodically formed and shed off from the catalytic substrate.

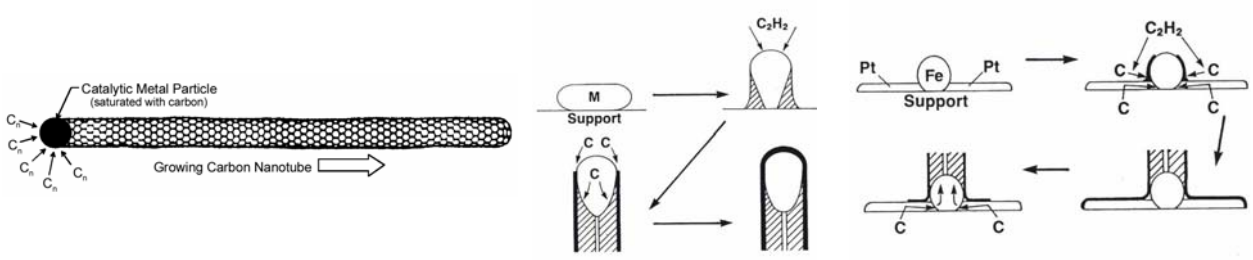

(a) Baker mechanism for CNT growth. **(b)** Particle at the tip. **(c)** Particle at the base.

Figure 3. CNT growth from catalyst particle. (Images used from other sources.)

Flame Synthesis Configurations

Fundamental studies of the scalar structure of a flame are best conducted in a flow field that is the simplest possible, facilitating data taking, analysis, and interpretation. Computational simulation of such a flame is straightforward and allows for meaningful comparisons between the experimental and computed results. It is also well known that the flame mode, i.e. premixed or non-premixed, can have a profound effect on nanoparticle formation, as for example in nano-catalysts for CNT growth, due to associated flame structures. As a result, we examine and compare synthesis in two specific quasi-one-dimensional, planar configurations, namely premixed stagnation point flow and non-premixed counterflow, where both aerosol catalyst and supported substrate methods are employed. Specifically, we examine the effects of fuel composition, flame temperature, inert addition, hydrogen addition, oxygen concentration, strain rate, and other controllable process parameters on nanoparticle encapsulation.

The axisymmetric, stagnation-point, fuel-rich premixed flame (Fig. 4) is formed by flowing reactants through a converging nozzle impinging onto a temperature-controlled substrate. The main fuel used is methane. Carbon-based growth can occur at the substrate if it is coated with a catalytic transition metal, e.g. Ni, Fe, or Co. Heat and radicals from the flame extract/reduce the requisite metal nanoparticles from the substrate, which serve as catalysts for CNT growth, characterized by adsorption, diffusion, and precipitation processes. Film thickness (e.g. CNT length in well-aligned growth) can be controlled by varying the deposition time, which is on the order of a few minutes for tens of microns of CNT length. Given the application, rather than having a catalytic substrate, we introduce metallocenes into the premixture, so that catalytic nanoparticles are homogeneously formed in the flow field due to a steep temperature gradient. Depending on the residence time, precursor loading, substrate temperature, and substrate material, CNTs can either form in the flow field and deposit on the substrate or grow continuously on the substrate after initial thermophoretic nanoparticle deposition. This flame geometry provides an excellent condition for uniform film growth, since all gradients are in the axial direction. Concurrently, the described setup allows for strategic control of the many process parameters involved. Moreover, our “flame CVD”-type process can produce high quality CNTs at atmospheric pressure, and is readily scalable similar to a spray coating process (e.g. in Fig. 4, the burner can be translated to cover large areas).

The opposed-jet counterflow non-premixed flame configuration provides various advantages for fundamental study. As seen in Fig. 5, the flame can be purposefully stabilized on the oxidizer side of the stagnation plane established between two converging nozzles. In this configuration, there is excellent control of pyrolysis effects. By mounting a substrate probe to a linear translation stage, CNT growth and characteristics can be investigated as function of axial position (corresponding to specific local conditions in temperature and species concentrations, i.e.

CO and C2's). Note that since the probe is on the fuel side, no oxygen is present, but plenty of carbon-based precursors are. In another study, aerosol catalyst synthesis can be realized by seeding the oxidizer (or fuel) stream with metallocenes, which homogeneously nucleate into catalytic nanoparticles, inducing CNT growth. This method has been shown to produce SWNTs.

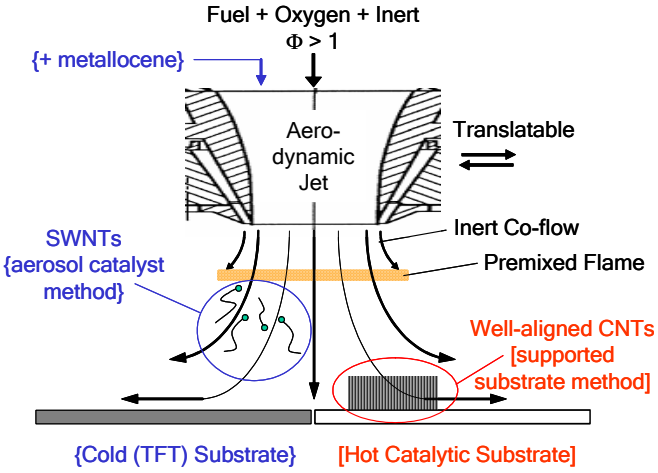

Figure 4. Premixed flame setup.

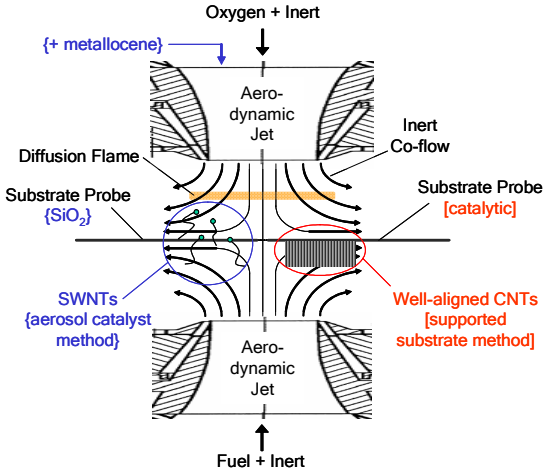

Figure 5. Diffusion flame setup.

To aid in scanning the parameter space, a unique flame configuration, the inverse jet diffusion flame, is employed in this work. Here the oxidizer is in the center, and fuel is on the outside; see Fig. 6. The net effect of this geometry is that post-flame species are largely comprised of pyrolysis vapors that have not passed through the oxidation zone. As such, soot formation processes, which compete with CNT formation routes, are more effectively separated from oxidation processes in inverse diffusion flames (IDFs), which also tend to soot less than normal diffusion flames (NDFs). Furthermore, the hydrocarbon and pyrolysis species (rich in Cn and CO) generated can be much greater in concentration than that practically achieved in premixed flames. The large characteristic thermal and chemical gradients characterizing flames are especially advantageous for determining CNT growth conditions in that a large parameter space of conditions can be found within a single flame. By probing a flame such as that shown in Fig. 6 at various heights, local flame structure conditions amenable for CNT growth are readily found. In comparison, systematic variation of parameters such as chemical species and temperature in a CVD reactor would be very time-consuming and tedious. Further utilization of advanced laser-diagnostics to determine the local in-situ temperature and gas-phase chemical species concentrations for given CNT morphologies and growth rates not only reveal fundamental mechanisms, but also establish "universal" conditions which should be directly applicable as specific operating conditions for other methods of synthesis.

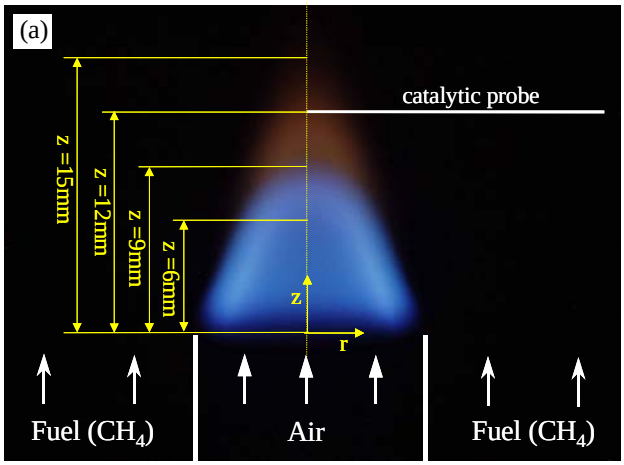

Figure 6. Methane inverse co-flow jet diffusion flame.

In-situ Laser-based Diagnostics

Advanced laser-based diagnostic techniques are employed to quantify the synthesis process. Gas-phase temperature measurements can made using spontaneous Raman spectroscopy (SRS) of N_2. Chemiluminescence imaging of acetylenic carbon provides an overall view of the combustion zones as well as spatial distribution information. For chemical species distributions, we utilize SRS to measure the concentrations of major species (e.g. N_2, O_2, H_2O, H_2, CO, C_2H_2), and LIF to measure the relative concentrations of important radical species (e.g. H, OH), as well as, the presence of gas-phase precursors (e.g. PAHs and C2s). At the same time, the vibrational modes (phonons) in the CNTs can be characterized by resonant Raman spectroscopy, with a spectrum that varies as a function of SWNT diameter. We utilize this technique in-situ to map zones of CNT growth, as well as identify characteristic SWNT diameters and CNT spatial distribution. As such, the flame can be adjusted for optimum growth rate, characteristics, and deposition morphology.

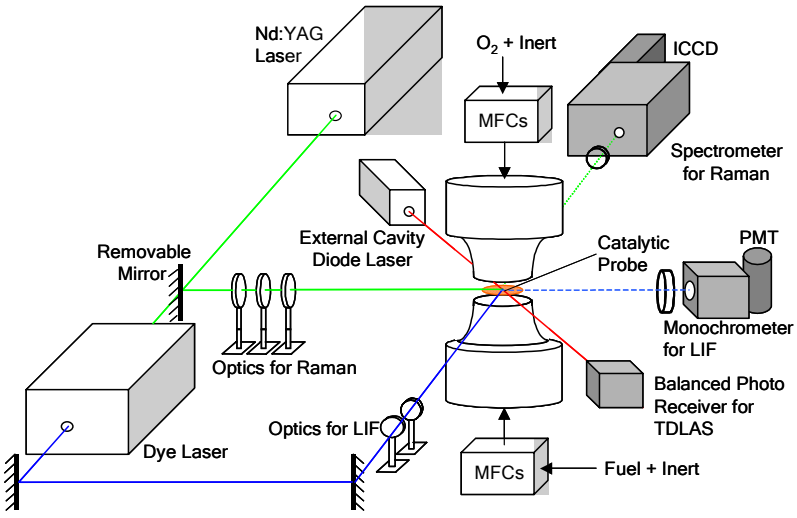

Figure 6. Laser-based diagnostics for flame synthesis.

Results from the Supported Catalyst Method using Metal Alloys

In general, transition metals (e.g. Ni, Co, and Fe) and their alloys have been used as catalysts for CNT growth. Bimetallic catalysts, such as alloys, are known to increase the yield of CNTs[8]. Alloys show a decrease in their melting temperature and an increase in the carbon solubility as compared to single metals[9]. Carbon solubilities for different metal alloys are different, as well as temperature-dependent. Figure 7(a) shows a TEM image of CNTs produced in our flame synthesis process where numerous metal catalyst nanoparticles, as indicated by the dark spheres, are encapsulated within single CNTs. Interestingly, and particularly important for the present work, X-ray energy-dispersive spectroscopy (XEDS) identifies that the elemental composition of the encapsulated nanoparticles is made up of not only the catalytic transition metal but also other elements from the alloy substrates during the synthesis process (see Fig. 7(b)). As such, our goal is to adjust local gas-phase conditions to maximize encapsulation of nanoparticles at a high and regular rate.

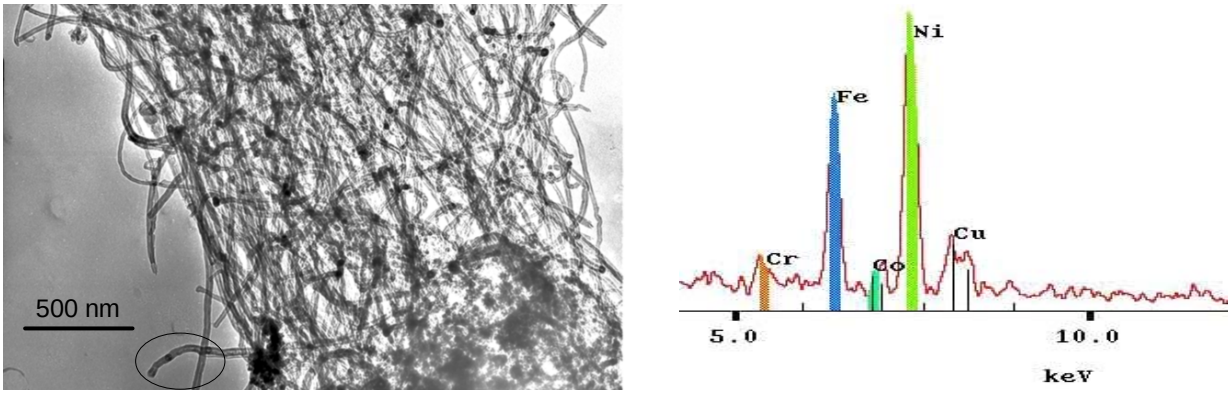

(a) TEM of CNTs with encapsulated nanoparticles. **(b)** XEDS Spectrum of catalyst nanoparticle.

Figure 7. CNT and catalyst nanoparticle properties of materials using flame synthesis.

Various morphologies of CNTs are grown catalytically on metal-alloy substrates of different compositions (i.e., Fe, Fe/Cr, Ni/Cu, Ni/Ti, Ni/Cr, Ni/Cr/Fe). Under favorable conditions, C_2 or CO species readily diffuse through catalyst nanoparticles and grow into CNTs. Vertically well-aligned CNTs with uniform diameter can be produced at specific locations in the flame structure, as seen in Fig. 8. Figure 9 presents characteristic counterflow synthesis flames, along with their corresponding flame structures, as predicted computationally using detailed chemical kinetics and transport and verified experimentally using spontaneous Raman spectroscopy (SRS) for gas-phase temperatures and major species concentrations (i.e. CH_4, C_2H_2, CO, H_2). As can be seen, the flames can be readily tailored. For example, Fig. 9(b) differs from Fig. 9(a) only by the acetylene concentration at the substrate probe, which directly affects CNT morphology and nanoparticle encapsulation, with the former characterized by entangled CNTs and the latter by well-aligned CNTs. As can be seen in Fig. 9(d), C_2H_2 mole fraction at the probe location is about 6 times higher for Flame#2 than Flame#1 (Fig. 9(c)), while gas-phase temperature and CO mole fraction remain about the same. Note that although there is a visible

soot layer in Fig. 9(b), the substrate probe is inserted into the non-sooty stagnation region, and the resulting CNT yield is unadulterated.

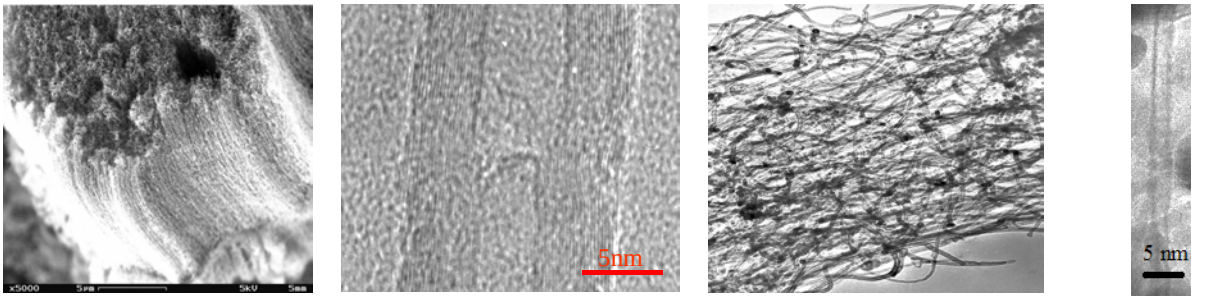

(a) Well-aligned CNTs (b) MWNT with hollow core (c) CNT bundles (d) SWNT

Figure 8. Carbon nanotubes (MWNTs and SWNTs) grown in our flame synthesis system.

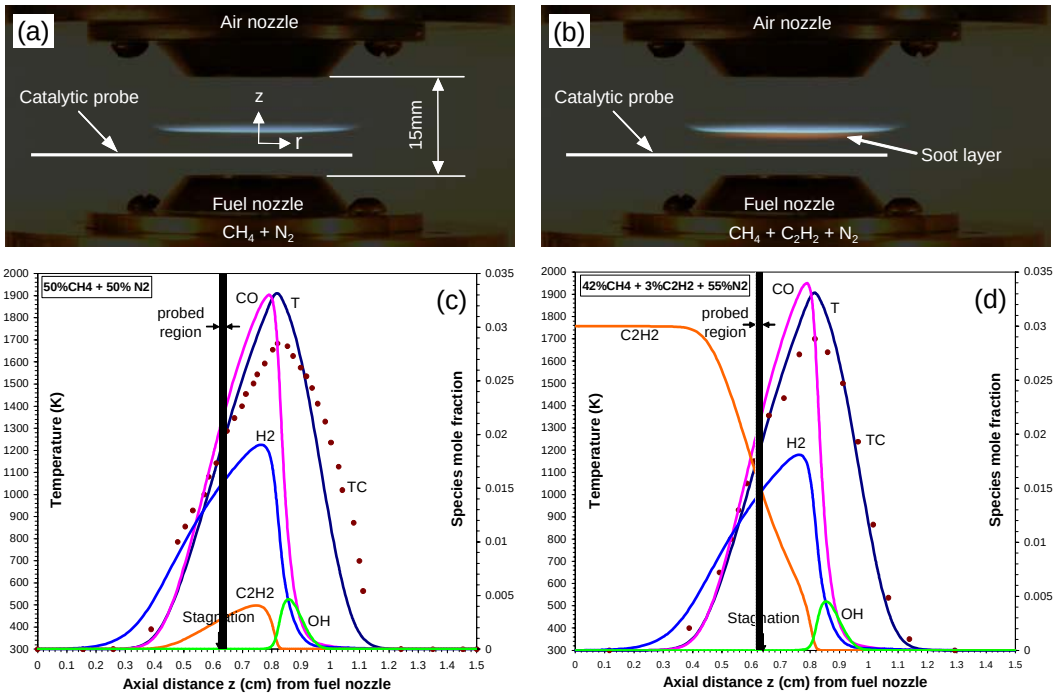

Figure. 9. Experimental setup for counterflow diffusion flame synthesis of CNTs: (a) Flame #1: methane as fuel and reagent, and (b) Flame #2: methane with acetylene addition. Corresponding flame structures for (a) and (b) are found below them, respectively. Thermocouple measurements (TC) assess actual substrate probe temperatures. Strain rate is $20s^{-1}$.

C_2H_2 addition is found to significantly affect the floating potential, as induced by flame-generated ions and electrons, for example on the Ni/Cr/Fe probe. As shown in Fig. 10, for the nanostructures grown in Flame#1 (Fig. 9(c)), the substrate floating potential is only -2mV, while for the nanostructures grown in Flame#2 (Fig. 9(d)), it is -14mV. The substrate floating potential produced in a different flame geometry (i.e. inverse co-flow, Fig. 6), but with the same local conditions as for Flame #2, is -24mV. The difference in induced voltages may be due to

differences in ion deposition rates from different probe temperatures. Nevertheless, our study shows that such electric potentials can significantly affect CNT alignment. Although applied potentials as small as a few tens of millivolts can develop an electric field exceeding 1000V/cm at the characteristic nanotube diameter, perhaps causing alignment, we do not observe alignment in the other metal alloys, even under applied voltage bias. As such, the density of catalytic nanoparticles formed is likely the key parameter, which allows for neighboring CNTs to provide vertical support for each other so that orderly growth perpendicular to the substrate occurs. Carbide induced breakup of the alloy surface to form catalyst nanoparticles responsible for CNT growth may be affected by C2 transport to the surface, as reflected by the induced voltage. XEDS of a single catalyst nanoparticle at the tip of a CNT grown from a Ni/Cr/Fe probe reveals that both Fe and Ni are present.

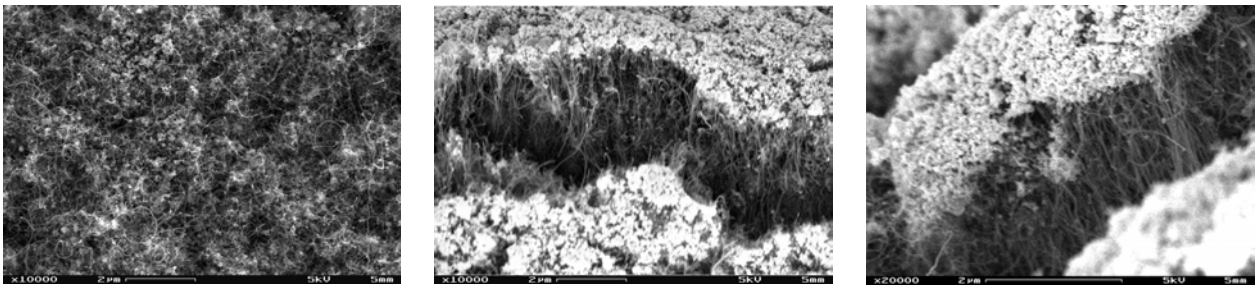

(a) Flame #1, counterflow FP = -2mV | (b) Flame #2, counterflow FP = -14mV | (c) Inverse Co-Flow FP = -24mV

Figure 10. C_2H_2 effect on CNT alignment (and substrate floating potential).

Re-inspecting the FESEM image of Figs. 10(b,c), it seems that a layer of densely packed nanoparticles of Ni-Fe-Cr composition is uniformly lifted off the surface of the probe, catalyzing aligned nanotube growth. As mentioned previously, the difference between entangled growth (Fig. 10(a)) and well-aligned growth (Figs. 10(b,c)) is likely due to the density of catalytic nanoparticles formed on the alloy surface. A high density of nanoparticles allows for neighboring CNTs to provide vertical support for each other so that orderly growth perpendicular to the substrate occurs. For alloys corresponding to well-aligned CNTs, TEM imaging verifies the particle-at-the-tip mechanism to prevail, where the dense morphology impedes transport of C-related species to the surface of the alloy substrate. Thus instances of nanoparticle encapsulation are rare for these cases. On the other hand, the results show that particle at the base mechanism is most favorable for repeated nanoparticle encapsulation. Sparse initial density of catalyst nanoparticles formed on the alloy substrate allows C2 and CO species to be readily transported to the alloy surface. Without neighboring support due to the large spacing between the particle-anchored CNTs, CNTs easily bend, growing in random directions. With HCs readily infiltrating the loose weave of CNTs to reach the alloy surface, continued carbide induced breakup of the alloy surface occurs, facilitating new nanoparticle formation, with the old nanoparticle shedding off and encapsulating within the continuously growing CNT.

Through dissociative adsorption, hydrocarbons supply elemental carbon to the metal alloy, where solvation of the adsorbed carbon produces a metal carbide phase as the carbon solubility for the metal alloy is exceeded. The metal carbide, which forms at the alloy surface, possesses sufficiently different lattice spacings than the surrounding metal phase, thus initiating

surface breakup and fragmentation (which occurs along surface defect sites and grain boundaries) generating potential catalyst particles. By tailoring the flame structure, we can supply C-related species at given rates to promote carbide formation favorable for well-spaced nanoparticle formation. Further manipulating the C_2H_2 to CO ratio should impact this, and is being studied. At the same time, ongoing study is being conducted on adjusting local gas-phase conditions to maximize encapsulation of nanoparticles with high aluminum content, at a high and regular rate using Al/(Fe, Co, Ni) alloys.

Results from the Supported Catalyst Method using Reduced Metal-Oxides

Among the various catalyst preparation methods, the *in-situ* reduction of solid solution can create catalytic nanoparticles needed for CNT growth. A well-crystallized solid solution has a low specific surface area, favoring the formation of metal particles of very small size, with low yield but high quality CNTs of high aspect ratio. Well-spaced CNTs on spinel-based substrates should favor particle-at-the- base growth mechanism, facilitating nanoparticle encapsulation. In this work, we report the catalytic synthesis of CNTs (containing MWNTs and SWNTs) in a soot-free counterflow diffusion methane/air flame by using catalysts (i.e. Ni, Co and Fe) prepared from *in situ* reduction of spinel solid solutions (i.e., $NiAl_2O_4$, $CoAl_2O_4$ and $ZnFe_2O_4$); see Fig. 11. We demonstrate the application of this processing route using flame synthesis under atmospheric pressure to produce CNTs encapsulating metal nanoparticles with Al content.

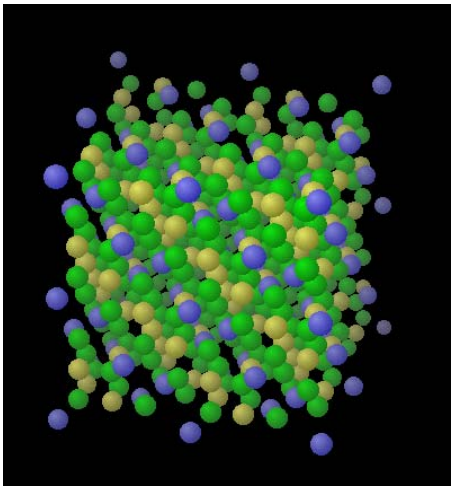

Spinels have a chemical formula of XY_2O_4 where Y is yellow, X is blue and O is green. It consists of a Y cation in the center of an oxygen octahedron and an X cation in the center of an oxygen tetrahedron

Figure 11. Ideal Spinel Crystal Structure.

All spinel powders are prepared by co-precipitation process. The specific spinels examined are: cobalt aluminate ($CoAl_2O_4$), nickel aluminate ($NiAl_2O_4$), and zinc ferrite ($ZnFe_2O_4$), with each spinel targeting one of the transition metals (e.g. Co, Ni, Fe) conducive for catalytic CNT growth, and with the first two containing aluminum. The as-prepared spinel powders are put into ethanol with a weight ratio of 20% spinel, and then ultrasonicated for 20 minutes to form a homogeneous suspension. This suspension is dropped onto the surface of a copper substrate and dried in air.

The three as-prepared spinel solid solution powders were analyzed by XRD, and their patterns are shown in Fig. 12. For the cobalt aluminate, all peaks are indexed to be $CoAl_2O_4$

spinel phase without impurities. For the nickel aluminate, although all the peaks corresponding to $NiAl_2O_4$ spinel phase are accounted for, the peaks are characteristically a bit wider than those for our $CoAl_2O_4$ sample, reflecting a smaller crystallization size and a poorer crystallization level. For zinc ferrite, all peaks can be attributed to the $ZnFe_2O_4$ spinel phase, and are very sharp showing the best crystallization level among the three solid oxide solutions.

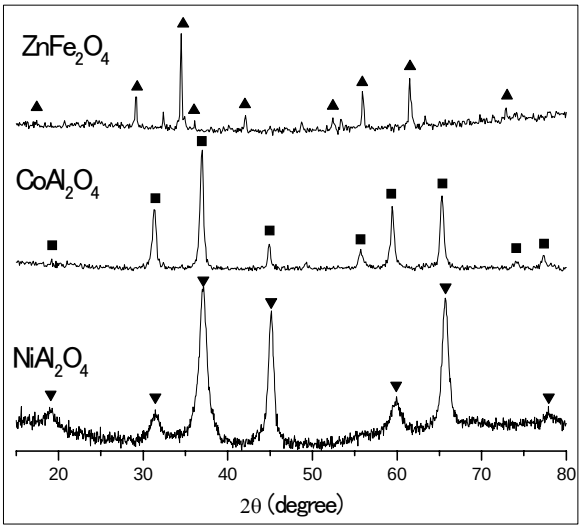

Figure 12. XRD patterns of as-prepared spinel solid solutions.

The experimental setup is that shown in Fig. 9(a). A spinel-coated copper substrate probe is inserted into the hydrocarbon-rich fuel side of the flow field. The as-grown carbon materials are investigated directly using field-emission scanning electron microscopy (FESEM) to assess CNT morphology. After ultrasonic treatment, low magnification transmission electron microscopy (TEM) and high-resolution TEM (HRTEM) characterize individual CNT and bundles.

The three spinel solid solutions, i.e., $NiAl_2O_4$, $CoAl_2O_4$ and $ZnFe_2O_4$, are examined under the same conditions to assess the quality and quantity of CNTs grown on them. The catalyst nanoparticles (Ni, Co and Fe) are obtained by *in situ* reduction in the flame structure by H_2[10] and CO[11] from their corresponding ion states in the three corresponding spinel solid solutions. The profiles of H_2 and CO are shown in Fig. 9(c). The catalyst nanoparticles extracted from the surface of the reduced grains serve to catalyze CNT growth, while those present in the interior of the grains remain inactive. Carbon precursors (e.g. CO and C_2H_2) readily undergo dissociative adsorption on these catalytic nanoparticles, diffusing to grow CNTs[12], with the nanoparticles either remaining attached to the solid solution surface, situated at the base of the growing CNT, or detaching from the surface and becoming situated at its tip.

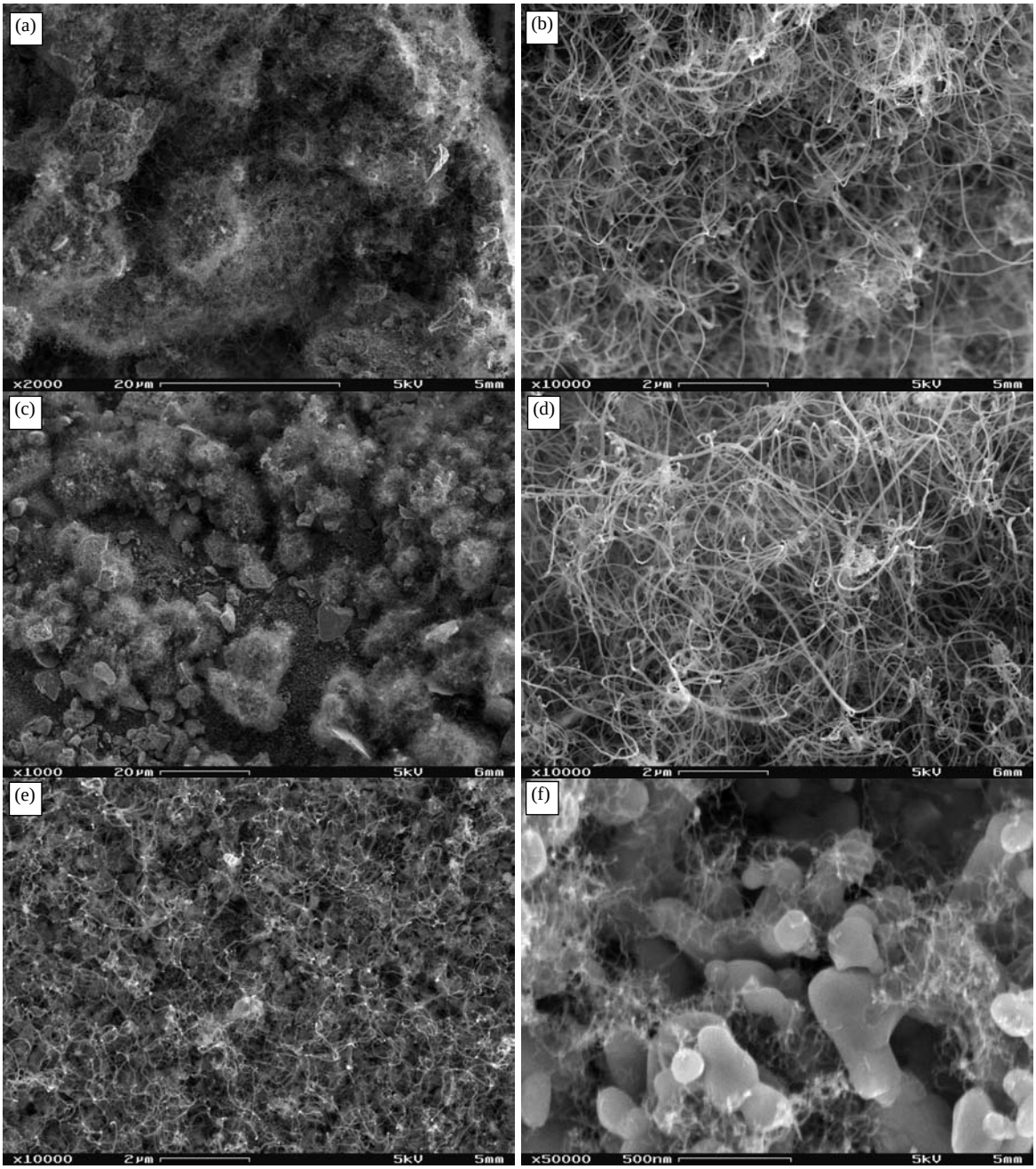

Figure 13. Typical FESEM images of CNTs grown from spinel solid solutions formed under the same flame conditions: (a) Low magnification image of CNTs from $NiAl_2O_4$. (b) High magnification image of CNTs covering a single reduced $NiAl_2O_4$ grain. (c) Low magnification image of CNTs from $CoAl_2O_4$. (d) High magnification image of CNTs covering a single reduced $CoAl_2O_4$ grain. (e) Low magnification image of CNTs from $ZnFe_2O_4$. (f) High magnification image of CNTs covering reduced $ZnFe_2O_4$ grains.

Figure 13 shows typical FESEM images of CNTs grown from the spinel solid solutions with extensive nanoparticle encapsulation. Figure 13(a) shows a low magnification image of CNTs grown from $NiAl_2O_4$, where all reduced grains are covered with densely packed CNTs at a significant yield. A closer look at the surface of a single reduced grain, as shown in Fig. 13(b),

reveals that it is covered uniformly and densely with CNTs arranged in long entangled bundles with diameters of 20~50 nm and lengths longer than 10μm. The encapsulated nanoparticles are clearly seen. The CNTs obtained from $CoAl_2O_4$ are similar to those from $NiAl_2O_4$, in terms of length, diameter, and yield, as shown in Fig. 13(c) (at low magnification) and in Fig. 13(d) (at higher magnification). Again, nanoparticle encapsulation is extensive. Noting that the magnification of Fig. 13(e) is the same as those of Figs. 13(b,d), the majority of CNTs produced from $ZnFe_2O_4$ are much thinner (< 15 nm) and shorter (~2μm), with a lower yield, than those produced from $NiAl_2O_4$ and $CoAl_2O_4$. The very high magnification FESEM image of Fig. 13(f) shows that the many of the CNTs from $ZnFe_2O_4$ are extremely fine in structure. TEM imaging and Raman spectroscopy reveal that a significant fraction are SWNTs with diameters of <5 nm, with correspondingly small encapsulated nanoparticles.

TEM presents the detailed structures of the as-grown CNTs. Figure 14(a) shows bundles of CNTs grown from $NiAl_2O_4$, whose diameters range from ~20-40 nm. As revealed by HRTEM (Fig. 14(b)), the synthesized materials are MWNTs with strong graphitic structure. For the same flame conditions, although not shown, similar MWNTs are produced in the $CoAl_2O_4$ system.

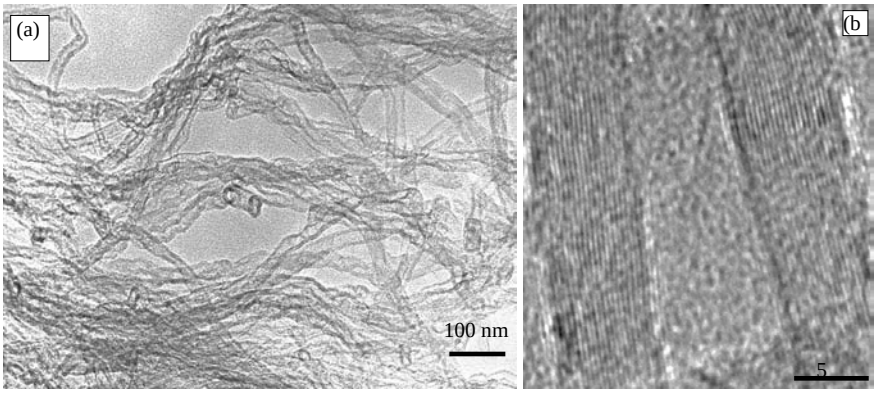

Figure 14. TEM images of CNTs from $NiAl_2O_4$.

Figure 15 reveals the composition of the encapsulated metal nanoparticles for the $NiAl_2O_4$ system. It appears that there is significant aluminum content; however it may be in the form of aluminum oxide, as the Al regions correspond to the O regions, as shown in Fig. 15(a). Nonetheless, Ni regions do not seem correlated with O regions. The future goal would be adjust conditions so that Al is present in non-oxide form as seemingly found for Ni, under the current conditions.

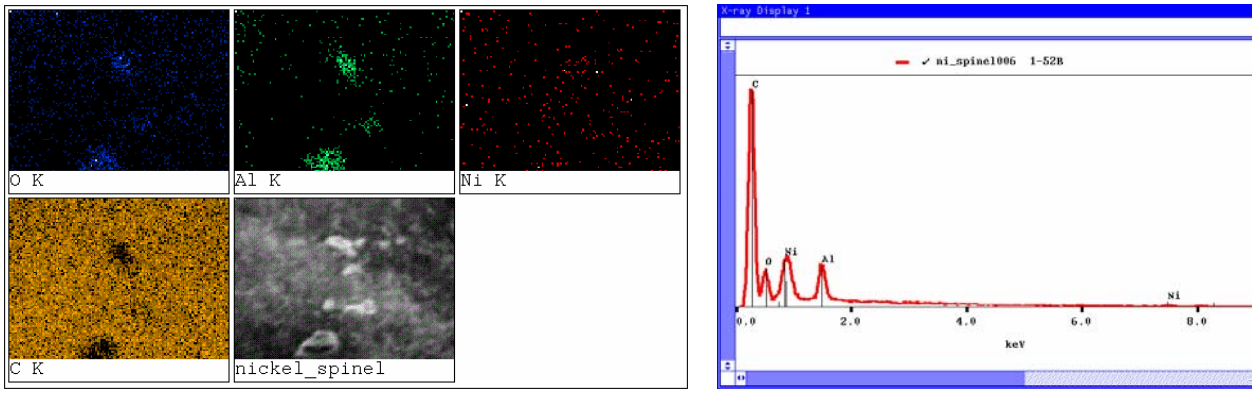

(a) XEDS mapping (b) XEDS

Figure 15. Encapsulated nanoparticle composition.

As observed from FESEM images (Fig. 13(f)), much thinner CNTs are obtained from $ZnFe_2O_4$. Examination under TEM (Fig. 16(a)) evinces that the outer diameters of the CNTs are less than 15 nm, along with similarly sized encapsulated nanoparticles; and the inset shows a SWNT with a diameter of around 3 nm. The large presence of SWNTs produced in the $ZnFe_2O_4$ system is further confirmed by Raman Spectroscopy (using a Renishaw System 1000 micro-Raman spectrometer), with laser excitation at two wavelengths, namely, 633 nm and 785 nm. In fact, as shown in Fig. 16(b), the SWNTs are of very small diameter. From the Radial Breathing Modes (RBM) frequencies collected at the corresponding excitations, the characteristic SWNT diameters are calculated to be 0.87 nm, 1.34 nm, 1.52 nm (from the RBM peak positions v (cm^{-1}) = 283, 184, and 163, respectively, due to 633 nm excitation), 0.84 nm, and 1.08 nm (from the RBM shifts peak positions v (cm^{-1}) = 293 and 228, respectively, due 785 nm excitation), by using the empirical relationship $d = 248/v$ [13,14], where $d(nm)$ indicates the nanotube diameter. Ongoing work involves introducing aluminum content into these very small nanoparticles.

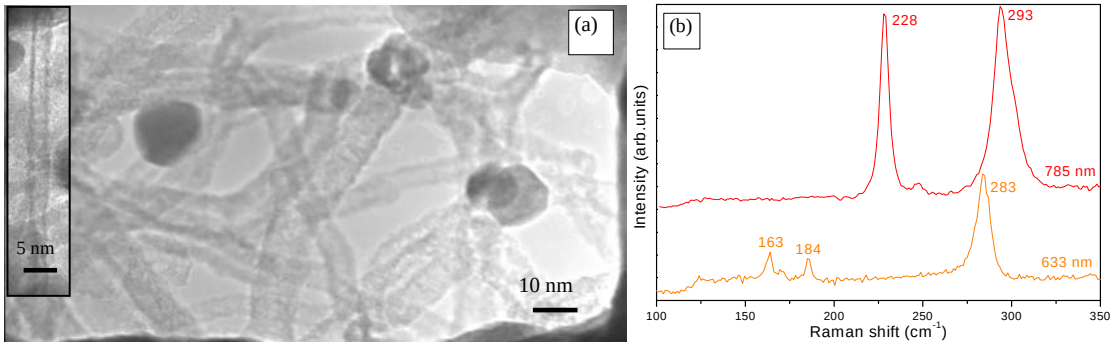

Figure 16. (a) TEM images of CNTs from $ZnFe_2O_4$. (b) Raman spectra of SWNTs from $ZnFe_2O_4$.

The large characteristic thermal and chemical gradients characterizing our flames are especially advantageous for determining CNT encapsulation growth conditions in that a large parameter space of conditions can be investigated within a single flame. The spinel solid solutions are tested at different axial z locations in the flame. No filamentous carbon (only amorphous carbon) is observed above z = 6.6mm, corresponding to the fuel side where the local

gas-phase temperature is ~1350K, despite increasing concentrations of carbon precursors such as CO and C_2H_2, reasonably in line with the observation reported that only some CNTs are formed at temperature close to 1340K. This is likely due to deactivation of the catalysts at such high temperatures. Figure 17 shows FESEM images of MWNTs grown from $NiAl_2O_4$ solid solution tested at three different axial *z* locations in the flame, where the gas-phase temperatures range from 1300K to 1000K with decreasing axial height. As can be seen in Figs. 17(a-c), there appear to be only slight differences in CNT diameters and lengths, but obvious differences in yields. Although the Ni nanoparticles reduced from solid solutions are active at the temperatures within this spanned range, the yield in Fig. 17(b) is the highest. Increasing the temperature increases the reduction yield and thus favors the formation of surface metal particles. More CNTs can be produced as long as the temperature is not too high to deactivate them. As such, the yield decrease in Fig. 17(a) is likely due to the onset of deactivation of the formed Ni nanoparticles at higher temperatures, whereas the decreased CNT yield in Fig. 17(c) may be attributed to the lower formation rate of Ni nanoparticles reduced from solid solution at lower temperatures. Below *z*= 5.8mm, where the local gas-phase temperatures are ~950K, CNTs are no longer observed, despite sufficient concentrations of CO and C_2H_2. This result likely corresponds to the lack of nanoparticle formation at these temperatures, in agreement with the observed required temperature (usually above 600^{o}C) for catalytic methods[15]. The temperature range conducive for CNT growth in our experiment is similar to that used in CVD[16,17,18]. Note from Fig. 9(c) that the TC-measured temperatures (corresponding to the probe temperatures) and gas-phase temperatures are approximately the same in the region of CNT formation. Similar trends are found for the $CoAl_2O_4$ and $ZnFe_2O_4$ solid solutions.

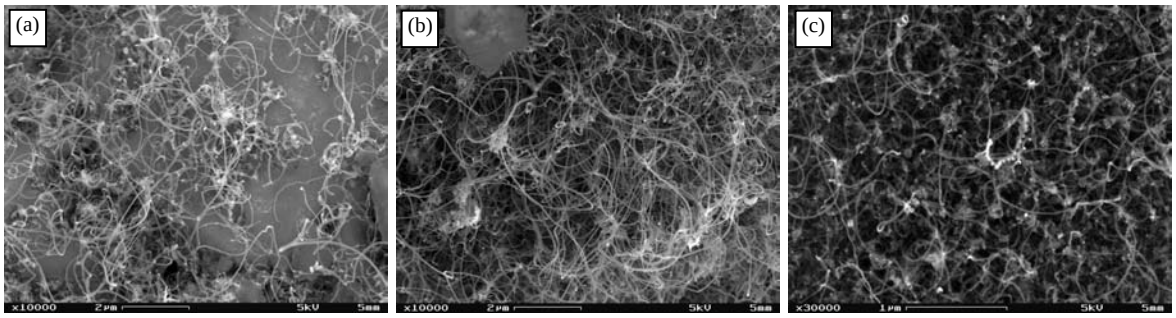

Figure 17. FESEM images of CNTs grown from $NiAl_2O_4$ at different axial z locations. (a) z=6.4mm. (b) z=6.2mm. (c) z=5.8mm

In summary, the degree of crystallization of the spinel affects the density (as well as chemical composition) of active catalytic nanoparticles formed. As seen above, local conditions, especially temperature, can have a similar effect. High H_2 concentration can increase the mobility of reduced metal nanoparticles, thus promoting coalescence and the formation of larger particles. Local CO to C_2H_2 ratio is an important parameter in that if a particle or site is not fully reduced, partial carbon solvation can take place during dissociative adsorption. The site can be deactivated if a carbide is formed. All of these factors contribute to the encapsulation of the catalytic nanoparticles into the growing CNTs.

Results from the Aerosol Catalyst Method using Ferrocene as Precursor

Running the experiment using a rich premixed flame seeded with ferrocene allows for growing CNTs in aerosol form with deposition onto a cold substrate in the stagnation point geometry. This method could be advantageous in depositing nanotubes, especially SWNTs, on substrates. We use a divergence stabilized methane-air premixed flame to grow CNTs encapsulated with nanoparticles. The mechanism and optimal conditions for CNT growth are investigated. Flame temperature, gas velocity, equivalence ratio, and catalyst particle size are varied throughout the experiment to determine the dependence of CNT formation on these factors.

Experimental setup for this experiment consists of a brass co-flow jet burner and a copper-aluminum substrate located 1.5 cm beneath the nozzle of the burner. The burner and the substrate are illustrated in Fig. 18(a). The flow system, which is controlled via mass flow controllers, along with precursor delivery unit, is showin Fig. 18(b). The temperature of the substrate is an important parameter becausee CNTs can grow at the substrate if the temperature is high enough. Since the purpose of the experiment is to generate CNTs in the aerosol, CNT growth on the substrate is suppressed by cooling.

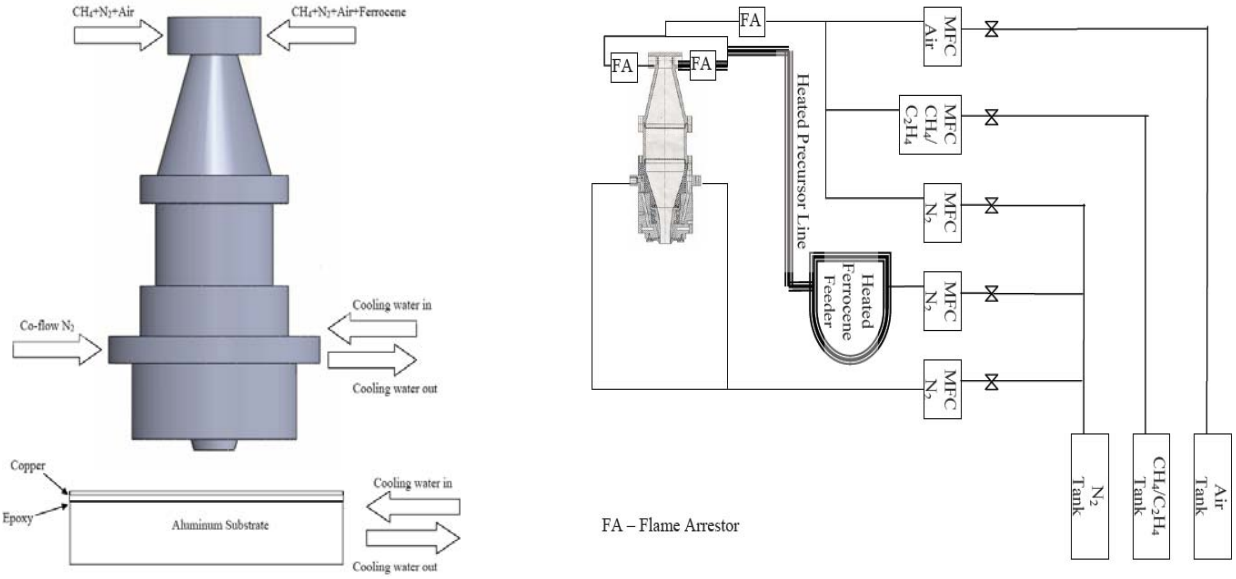

(a) Burner and substrate. (b) Flow system.

Figure 18. Experimental setup.

Figure 19 shows TEM images of the as produced nanomaterials from rich methane / air stagnation flames with ferrocene seeding. There is significant catalyst nanoparticle production, encased within carbon material, namely CNTs. Resonant Raman spectroscopy of the material shows significant SWNTs encapsulating the nanoparticles, as given in Fig. 20

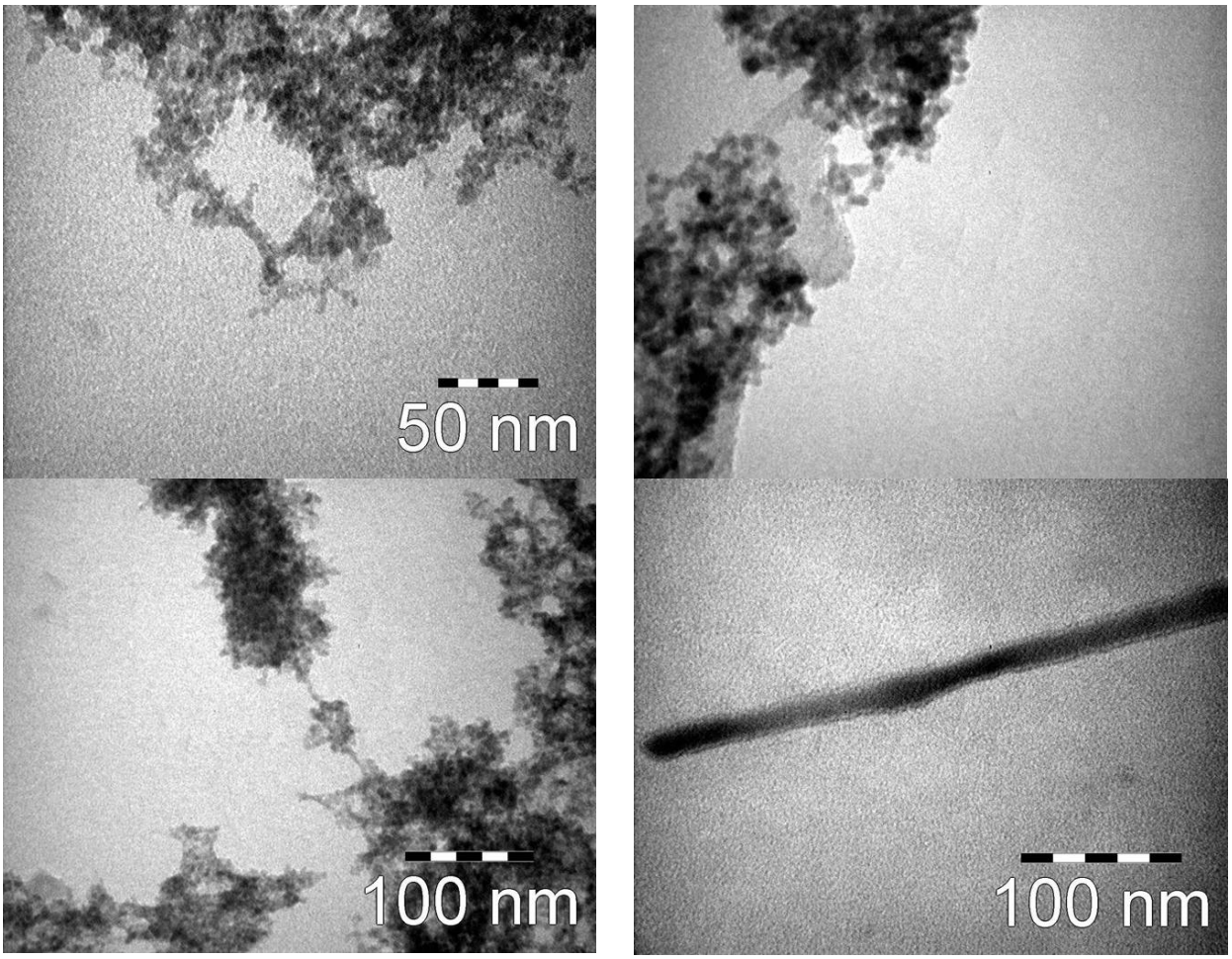

Figure 19. As produced nanomaterials from premixed stagnation flame.

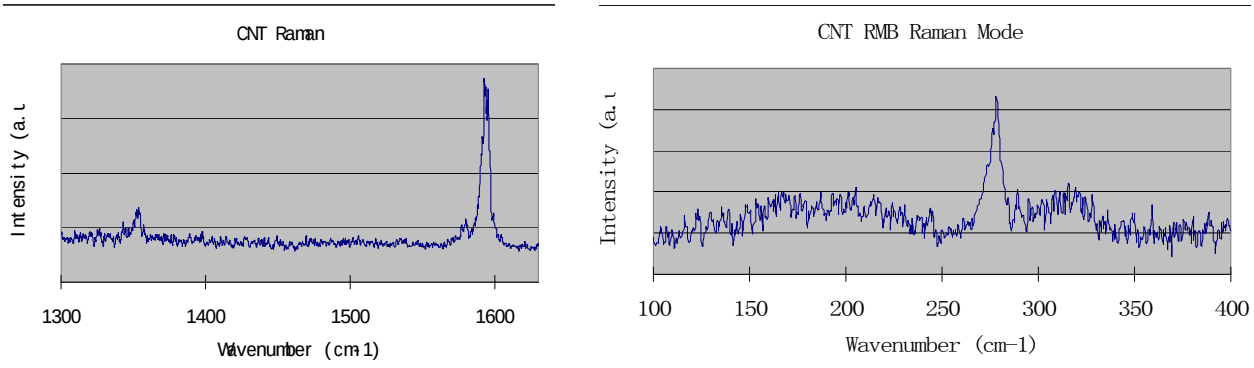

(a) G and D bands show graphitic material surrounding iron/iron-oxide nanoparticles.

(b) Radial breathing mode peak corresponds to SWNTs ~1nm diameter.

Figure 20. Resonant Raman spectroscopy showing SWNTs.

The results show that CNTs can also limit the particle size, especially if SWNTs are produced. On-going research resides on producing encapsulated nanoparticles with Al content.

Plasma Synthesis for Al Nanostructures

Utilizing a stagnation point geometry, plasma synthesis allows production of the aluminum nanostructures themselves; see Fig. 21. We employ a small-scale inductively-coupled RF-plasma system (2kW), whereby axial precursor (gaseous or liquid) injection enables good control of precursor residence time as the precursors pass down the center of the plasma. The laboratory-scale system is characterized by a well-defined laminar flow field. The setup consists of a plasma torch and encompassing chamber, radio frequency power supply, matching network, plasma gas, cooling water, precursor feeder, exhaust gas cleaning, and vacuum pumping system. An advantage of the inductively coupled plasma design is that the nozzle/cathode materials do not contaminate the powder being produced. Inductively coupled plasmas have been used in materials processing for melting and deposition of metals and ceramics, as well as for plasma synthesis of ultrafine powders of high purity. The absence of an electrode makes the operation easy with a wide range of gas input at atmospheric or low-pressure conditions.

In the axisymmetric, stagnation-point plasma geometry (Fig. 21), the plasma jet, seeded with chemical precursor vapor (e.g. aluminum sec butoxide), impinges onto a cold substrate. Liquid precursors are either vaporized and entrained into a carrier gas (e.g. nitrogen, argon) via a bubbling unit or pumped through a nebulizer into a spray chamber and delivered into the plasma as a gas or an aerosol, respectively. The chemical precursors vaporize and dissociate in the hot plasma, and then undergo nucleation, growth, chemical reactions, and quenching upon reaching the substrate.

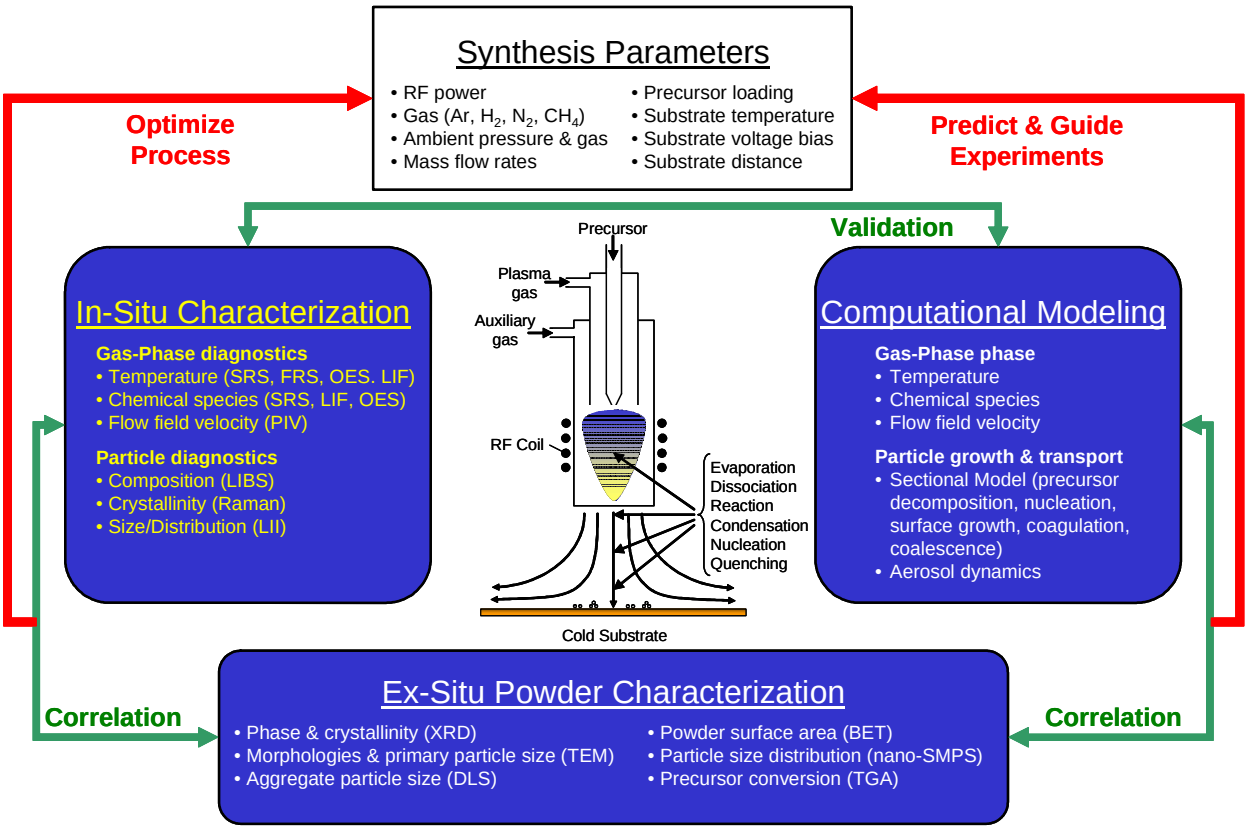

Figure 21. Concept diagram the optimized plasma synthesis of nanomaterials.

Figure 22 shows the as-synthesized material from the plasma reactor. Aluminum nanopowder is readily synthesized from ASB, as seen from the XRD pattern. At the same time, Raman spectroscopy indicates that it is encased in carbonaceous material, likely graphitic, by using a methane carrier gas. Such a CNT producing mechanism would likely be skullcap, rather than catalytic.

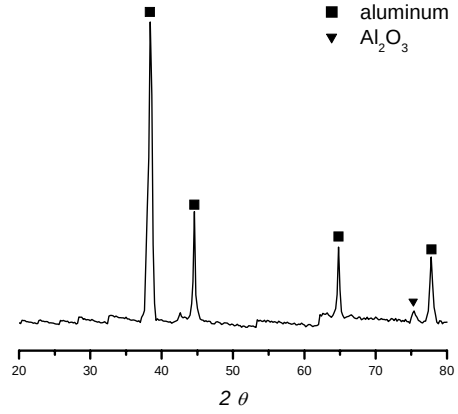

- Methane carrier gas
- Aluminum sec butoxide (ASB) seeding
- G and D bands → fullerenes, skullcap mechanism?

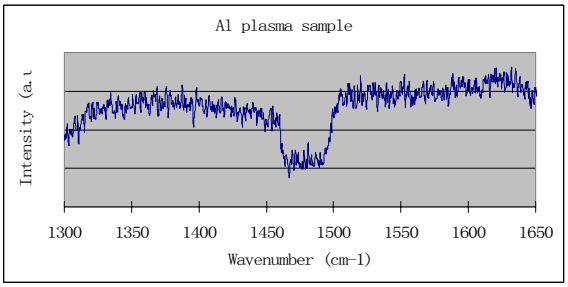

Figure 22. Materials synthesized in plasma reactor.

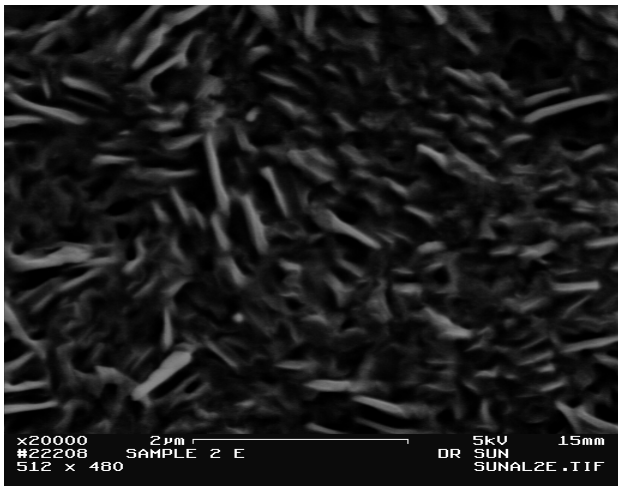

Figure 23. Aluminum nanostructures.